Nonlin. Processes Geophys. Discuss., doi:10.5194/npg-2017-17, 2017
Manuscript under review for journal Nonlin. Processes Geophys.
Discussion started: 25 April 2017

Nonlinear Processes in Geophysics
Discussions
Open Access
EGU

Multistable Slip of a One-degree-of-freedom Spring-slider Model in the Presence of Thermal-pressurized Slip-weakening Friction and Viscosity

Jeen-Hwa Wang
Institute of Earth Sciences, Academia Sinica
P.O. Box 1-55, Nangang, Taipei, TAIWAN
e-mail: jhwang@earth.sinica.edu.tw

Abstract This study is focused on multistable slip of earthquakes based on a one-degree-of-freedom slider-slider model in the presence of thermal-pressurized slip-weakening friction and viscosity by using the normalized equation of motion of the model. The major model parameters are the normalized characteristic displacement, U_c, of the friction law and the normalized viscosity coeficient, η, between the slider and background plate. Analytic results at small slip suggest that there is a solution regime for η and γ ($=1/U_c$) to make the slider slip steadily. Numerical simulations exhibit that the time variation in normalized velocity, V/V_{max} (V_{max} is the maximum velocity), obviously depends on U_c and η. The effect on the amplitude is stronger due to η than due to U_c. In the phase portrait of V/V_{max} versus the normalized displacement, U/U_{max} (U_{max} is the maximum displacement), there are two fixed points. The one at large V/V_{max} and large U/U_{max} is not an attractor; while that at small V/V_{max} and small U/U_{max} can be an attractor for some values of η and U_c. When $U_c<0.55$, unstable slip does not exist. When $U_c\geq0.55$, U_c and η divide the solution domain into three regimes: stable, intermittent, and unstable (or chaotic) regimes. For a certain U_c, the three regimes are controlled by a lower bound, η_l, and an upper bound, η_u, of η. The values of η_l, η_u, and η_u-η_l all decrease with increasing U_c, thus suggesting that it is easier to yield unstable slip for larger U_c than for smaller U_c or for larger η than for smaller η. When $U_c<1$, the Fourier spectra calculated from simulation velocity waveforms exhibit several peaks, thus suggesting the existence of nonlinear behavior of the system. When $U_c>1$, the related Fourier spectra show only

one peak, thus suggesting linear behavior of the system.

Key Words: Multistable slip, one-degree-of-freedom spring-slider model, displacement, velocity, thermal-pressurized slip-weakening friction, viscosity

1. Introduction

The earthquake ruptures consist of three steps: nucleation, dynamical propagation, and arrest. Due to the lack of a comprehensive model, a set of equations to completely describe fault dynamics has not yet been established, because earthquake ruptures are very complicated. Nevertheless, some models, for instance the crack model and dynamical lattice model, have been developed to approach fault dynamics. Several factors will control earthquake ruptures (see Wang, 2016b; and cited references herein), including at least brittle-ductile fracture rheology, normal stress, re-distribution of stresses after fracture, fault geometry, friction, seismic coupling, pore fluid pressure, elastohydromechanic lubrication, thermal effect, thermal pressurization, and metamorphic dehydration. A general review can be seen in Bizzarri (2009). Among the factors, friction and viscosity are two important ones in controlling faulting.

Burridge and Knopoff (1967) proposed a one-dimensional spring-slider model (abbreviated as the 1-D BK model henceforth) to approach fault dynamics. Wang (2000, 2012) extended this model to a two-dimensional version. The two models and their modified versions have been long and widely applied to simulate the occurrences of earthquakes (see Wang, 2008, 2012; and cited references therein). In the followings, the one-, two-, three-, few-, and many-body models are used to represent the one-, two-, three-, few-, and many-degree-of-freedom spring-slider models, respectively. The few-body models have been long and widely used to approach faults (Turcotte, 1992)

Since the commonly-used friction laws are nonlinear, the dynamical model itself could behave nonlinearly. A nonlinear dynamical system can exhibit chaotic behaviour under some conditions (Thompson and Stewart, 1986; Turcotte, 1992). This means that the system is highly sensitive to initial conditions (SIC) and thus a small difference in initial conditions, including those caused by rounding errors in numerical computation, yields widely diverging outcomes. This indicates that long-term prediction is impossible in general, even though the system is deterministic,

Nonlin. Processes Geophys. Discuss., doi:10.5194/npg-2017-17, 2017
Manuscript under review for journal Nonlin. Processes Geophys.
Discussion started: 25 April 2017

67 meaning that its future behavior is fully determined by their initial conditions, without
68 random elements. This behavior is known as (deterministic) chaos (Lorenz, 1963).
69 An interesting question is: Can a simple few-body model with total symmetry
70 make significant predictions for fault behavior? Gu et al. (1984) first found some
71 chaotically bounded oscillations based on a one-body model with rate- and state-
72 dependent friction. Perez Pascual and Lomnitz-Adler (1988) studied the chaotic
73 motions of coupled relaxation oscillators. Related studies have been made based on
74 different spring-slider models: (1) a one-body model with rate- and state-dependent
75 friction (e.g., Gu et al., 1984; Belardinelli and Belardinelli, 1996; Ryabov and Ito,
76 2001; Erickson et al., 2008, 2011; Kostić et al., 2013); (2) a one-body model with
77 velocity-weakening friction (e.g., Brun and Gomez, 1994); (3) a one-body model with
78 slip-weakening friction (e.g., Wang, 2016a,b); (4) a two-slider model with simple
79 static/dynamic friction (e.g., Nussbaum and Ruina, 1987; Huang and Turcotte, 1990);
80 (5) a two-body model with velocity-dependent friction (e.g., Huang and Turcotte,
81 1992; de Sousa Vieira, 1999; Galvanetto, 2002); (6) a two-body model with rate- and
82 state-dependent friction (e.g., Abe and Kato, 2013); (7) a two-body model with
83 velocity-weakening friction (Brun and Gomez, 1994); (8) a two-body model with
84 slip-weakening friction (e.g., Wang, 2017); (9) many-body model with velocity-
85 weakening friction (e.g., Carlson and Langer, 1989; Wang, 1995, 1996); and (10)
86 one-body quasi-static model with rate- and state-dependent friction (e.g., Shkoller and
87 Minster, 1997). Results suggest that predictions for fault behaviour are questionable
88 due to the possible presence of chaotic slip.
89 The frictional effect on earthquake ruptures has been widely studied as
90 mentioned above. However, the studies of viscous effect on earthquake ruptures are
91 rare. The viscous effect mentioned in Rice et al. (2001) was just an implicit factor
92 which is included in the evolution effect of friction law. In this work, I will investigate
93 the effects of thermal pressurized slip-weakening friction and viscosity on earthquake
94 ruptures and the generation of unstable (or chaotic) slip based on a one-body model.
95
96 **2. MODEL**
97 **2.1 One-body Model**
98 Fig. 1 shows the one-body model whose equation of motion is:
99
100 $$md^2u/dt^2=-K(u-u_o)-F(u,v)-\Phi(v), \quad (1)$$

where m is the mass of the slider, u and v (=du/dt) are, respectively, the displacement and velocity of the slider, u_o is the equilibrium location of the slider, K is the spring constant, F is the frictional force between the slider and the background and a function of u or v, and Φ is the viscous force between the slider and the background and a function of v. The slider is pulled by a driving force F_D due to the moving plate with a constant driving velocity, v_p, through a leaf spring of strength, K. Hence, the driving force is $F_D=Kv_pt$ and thus $u_o=v_pt$. When F_D is slightly larger than the static frictional force, F_o, friction changes from static friction strength to dynamic one and thus the slider moves.

2.2 Viscosity

Jeffreys (1942) first emphasized the importance of viscosity on faulting. Frictional melts in faults depend on temperature, pressure, water content, and etc. (Turcotte and Schubert, 1982) and can yield viscosity on the fault plane (Byerlee, 1968). Rice et al. (2001) discussed that rate- and state-dependent friction in thermally activated processes allows creep slippage at asperity contacts on the fault plane. Scholz (1990) suggested that the friction melts would present significant viscous resistance to shear and thus inhibit continued slip. However, Spray (1993, 1995, 2005) stressed that the frictional melts possessing low viscosity could generate a sufficient melt volume to reduce the effective normal stress and thus act as fault lubricants during co-seismic slip. His results show that viscosity remarkably decreases with increasing temperature. For example, Wang (2011) assumed that quartz plasticity could be formed in the fault zone when T>300 ^oC after faulting and it would lubricate the fault plane at higher T and yield viscous stresses to resist slip at lower T. From numerical simulations, Wang (2007, 2016b, 2017) stressed the viscous effect on faulting. Noted that several researchers (Knopoff et al., 1973; Cohen, 1979; Xu and Knopoff, 1994; Knopoff and Ni, 2001; Dragoni and Santini, 2015) took viscosity as a factor in causing seismic radiation to reduce energy during faulting.

The viscosity coefficient, υ, of rocks is mainly controlled by temperature, T. An increase in T will yield partial melting of rocks and thus the viscosity coefficient, υ, first is increased, then reaches the largest value at a particular T, and finally decreases with increasing T The relation between υ and T can be described by the following equation (e.g., Turcotte and Schubert, 1982): $\upsilon=\upsilon_o\exp[(E_o+pV_a/RT)]$ where υ_o is the

Nonlin. Processes Geophys. Discuss., doi:10.5194/npg-2017-17, 2017
Manuscript under review for journal Nonlin. Processes Geophys.
Discussion started: 25 April 2017

largest viscosity at low ambient T of an area, E_o is the activation energy per mole, p is the pressure, V_a is the activation volume per mole, and R is the universal gas constant ($E_o/R \approx 3\times10^4$ K). Obviously, υ decreases with increasing T. This is particularly remarkable in regions of high confining pressure. On the other hand, Diniega et al. (2013) assume that υ exponentially depends on temperature: $\upsilon \sim e^{\beta(1-T^*)}$, where β is a constant and $T^*= (T-T_C)/(T_H-T_C)$ is a dimensionless temperature within a temperature range of T_C to T_H. The value of υ increases with T* when T*<1 and decreases with increasing T* when T*>1. Wang (2011) inferred that in the major slip zone<0.01 m of the 1999 M_s7.6 Chi-Chi, Taiwan, earthquake, T(t) in the fault zone at a depth of 1111 m increased from ambient temperature $T_a \approx 45$ ^oC at t=0 s to peak temperature T_{peak}=1135.1 ^oC at t=~2.5 s. T(t) began to decrease after t=2.5 s and dropped to 160 ^oC at t=195 s. This yields a change of viscosity in the fault zone.

The description about the physical models of viscosity can be found in several articles (Jaeger and Cook, 1977; Cohen, 1979; Hudson, 1980; Wang, 2016b). A brief description is given below. For many deformed materials, there are elastic and viscous components. The viscous component can be modeled as a dashpot such that the stress–strain rate relationship is: $\sigma=\upsilon(d\varepsilon/dt)$ where σ and ε are the stress and the strain, respectively. Two simple models (shown in Fig. 2) commonly used to describe the viscous materials are the Maxwell model and the Kelvin-Voigt model (or the Voigt model). The first one can be represented by a purely viscous damper (denoted by "D") and a purely elastic spring (denoted by "S") connected in series,. Its constitution equation is: $d\varepsilon/dt=d\varepsilon_D/dt+d\varepsilon_S/dt=\sigma/\upsilon+E^{-1}d\sigma/dt$ where E is the elastic modulus and $\sigma=E\varepsilon$. The constitutive relation of the second model is: $\sigma(t)=E\varepsilon(t)+\upsilon d\varepsilon(t)/dt$.

For the Maxwell model, the strain will increase, without a upper limit, with time; while the Kelvin-Voigt model the strain will increases, with a upper limit, with time. Wang (2016b) assumed that the latter is more appropriate than the former to be applied to the seismological problems as suggested by Hudson (1980). Hence, the Kelvin-Voigt model is taken in this study. To simplify the problem, only a constant viscosity is considered below. The viscous stress at the slider is represented by $-\upsilon v$.

However, it is not easy to directly implement viscosity in a dynamical system as used in this study. Wang (2016b) represented the viscosity coefficient in an alternative way. Viscosity leads to the damping of oscillations of a body in viscous fluids. The damping coefficient, η, depends on the viscosity coefficient, υ, and the linear

Nonlin. Processes Geophys. Discuss., doi:10.5194/npg-2017-17, 2017
Manuscript under review for journal Nonlin. Processes Geophys.
Discussion started: 25 April 2017

dimension, R, of the body in a viscous fluid. According to Stokes' law, the η of a sphere of radius R in a viscous fluid of υ is $\eta=6\pi R\upsilon$ (cf. Kittel et al., 1968). In order to simplify the problem, the damping coefficient is taken in this study. Hence, the viscous force is $\Phi=\eta v$. Noted that the unit of η is $N(m/s)^{-1}$.

2.3 Friction caused by thermal pressurization

Numerous factors can affect friction (see Wang, 2009, 2016b; and cited references herein). When fluids are present and temperature changes in faults, thermal pressurization will yield resistance on the fault plane and thus play a significant role on earthquake rupture (Sibson, 1973; Lachenbruch, 1980; Chester and Higgs, 1992; Fialko, 2004; Fialko and Khzan, 2005; Bizzari and Cocco, 2006a,b; Rice, 2006; Wang, 2000, 2006, 2009, 2011, 2013, 2016b, 017; Bizzarri, 2010; Bizzarri, 2011a,b).

Rice (2006) proposed two end-members models for thermal pressurization: the adiabatic-undrained-deformation (AUD) model and slip-on-a-plane (SOP) model. He also obtained the shear stress-slip functions caused by the two models. The first model corresponds to a homogeneous simple shear strain ε at a constant normal stress σ_n on a spatial scale of the sheared layer that is broad enough to effectively preclude heat or fluid transfer. The second model shows that all sliding is on the plane with $\tau(0)= f(\sigma_n-p_o)$ where p_o is the pore fluid pressure on the sliding plane (y=0). For this second model, heat is transferred outwards from the fault plane. Although the stress $\tau_{sop}(u)$ also shows slip-weakening (Wang, 2009), the SOP model is not appropriate in this study because of the request of a constant velocity for this model.

The shear stress-slip functions, τ(u), caused by the AUD model is:

$$\tau_{aud}(u)= f(\sigma_n-p_o)\exp(-u/u_c). \quad (3)$$

The parameters u_c is the characteristic displacements associated with the thickness and some physical properties of fault zone. The stress $\tau_{aud}(u)$ displays exponentially with u and thus exhibits slip-weakening friction. Based on the AUD model, Wang (2009) proposed a simplified slip-weakening friction law (denoted by the TP law hereafter): $F(u)=F_o\exp(-u/u_c)$, where F_o is the static frictional force, to study seismic efficiency. Wang (2016b, 2017) applied the law to simulate slip of one-body and two-body spring-slider models. Fig. 3 exhibits F(u) versus u for five values of u_c, i.e., 0.1, 0.3, 0.5, 0.7, and 0.9 m. The friction force decreases with increasing u and it

Nonlin. Processes Geophys. Discuss., doi:10.5194/npg-2017-17, 2017
Manuscript under review for journal Nonlin. Processes Geophys.
Discussion started: 25 April 2017

decreases faster for smaller u_c than for larger u_c. Meanwhile, the force drop decreases with increasing u_c. For small u, $\exp(-u/u_c)$ can be approximated by $1-u/u_c$ (Wang, 2016a,b, 2017). The parameter u_c^{-1} is almost the decreasing rate, γ, of friction force with slip at small u. Small (large) u_c is related to large (small) γ.

2.4. Predominant Frequency and Period of the System

To conduct marginal analyses of slip of one-body model with friction, Wang (2016b) used the friction law: $F(u)=F_o-\gamma u$. His results show that the natural periods are $T_o=2\pi/(K/m)^{1/2}$ when friction and viscosity are excluded and

$$T_n=T_o/[1-T_o^2(\eta^2+4m\gamma)/(4\pi m)^2]^{1/2}. \quad (4)$$

when friction and viscosity are included. Clearly, T_n is longer than T_o. Eq. (4) shows that T_n increases with η and γ, thus indicating that friction and viscosity both lengthen the natural period of the system.

3. Normalization of Equation of Motion

Substituting the TP law and the linear viscous law into Eq. (1) leads to

$$md^2u/dt^2=-K(u-u_o)-F_o\exp(-u/u_c)-\eta v. \quad (5)$$

To simplify numerical computations, Eq. (5) is normalized based on the following normalization parameters: $D_o=F_o/K$, $\omega_o=(K/m)^{1/2}$, $\tau=\omega_o t$, $U=u/D_o$, $U_c=u_c/D_o$, and $\Gamma_D=F_D/K$. This gives $du/dt=[F_o/(mK)^{1/2}]\, dU/d\tau$, $d^2u/dt^2=(F_o/mK)d^2U/d\tau^2$. The driving velocity becomes $V_p=v_p/D_o\omega_o$ Hence, the normalized acceleration and velocity are, respectively, $A=d^2U/d\tau^2$and $V=dU/d\tau$. The phase ωt is replaced by $\Omega\tau$, where $\Omega=\omega/\omega_o$ is the dimensionless angular frequency. Note that $\eta/(mK)^{1/2}$ is simply denoted by η below. Clearly, all normalization parameters are dimensionless. Hence, Eq. (5) becomes:

$$d^2U/d\tau^2=-U-\eta dU/d\tau-\exp(-U/U_c)+\Gamma_D. \quad (6)$$

When $F_D=v_p t$ or $\Gamma_D=V_p\tau$, Eq. (6) is transformed to a set of three first-order

Nonlin. Processes Geophys. Discuss., doi:10.5194/npg-2017-17, 2017
Manuscript under review for journal Nonlin. Processes Geophys.
Discussion started: 25 April 2017

Nonlinear Processes in Geophysics
Discussions
Open Access
EGU

differential equations by defining $x=U/U_c$, $y=V/V_p$, and $z=-U+V_p\tau-\eta V_p y_\tau$ ($y_t=dy/d\tau$):

$$x_\tau=(V_p/U_c)y \tag{7a}$$

$$y_\tau=(z-e^{-x})/V_p, \tag{7b}$$

$$z_\tau=V_p(1-y-\eta y_\tau). \tag{7c}$$

As $x<<1$, $e^{-x}\approx 1-x$ and thus Eq. (7b) can be approximated by $y_\tau\approx(z-1+x)/V_p$. The condition of $x<<1$ shows $U/U_c<<1$. Differential of this equation leas to $y_{\tau\tau}\approx(z_\tau+x_\tau)/V_p$, where $y_{\tau\tau}=d^2y/d\tau^2$. Substituting Eqs. (7a) and (7b) into this equation gives

$$y_{\tau\tau}+\eta y_\tau+(1-1/U_c)y=1. \tag{8}$$

The homogeneous equation of Eq. (8) is

$$y_{\tau\tau}+\eta y_\tau+(1-1/U_c)y=0. \tag{9}$$

Let the general solution be $y\sim e^{\lambda\tau}$. This leads to $[\lambda^2+\eta\lambda+(1-/U_c)]y=0$ or

$$\lambda^2+\eta\lambda+(1-/U_c)=0. \tag{10}$$

The solutions of Eq. (10) are

$$\lambda_\pm=-\eta/2\pm[\eta^2-4(1-1/U_c)]^{1/2}/2. \tag{11}$$

The term $-\eta/2$ of Eq. (11) leads to $e^{-\lambda/2}$ which yields attenuation of y. Define $D(\eta,1/U_c)$ to be $\eta^2-4(1-1/U_c)$. As mentioned above, U_c^{-1} is the normalized decreasing rate of friction, Γ, at $U=0$. Fig. 4 shows the plot of η versus $1/U_c$ and thus exhibits the root structure of the system. Because $\eta>0$ and $U_c>0$, only the plot in the first quadrant is

Nonlin. Processes Geophys. Discuss., doi:10.5194/npg-2017-17, 2017
Manuscript under review for journal Nonlin. Processes Geophys.
Discussion started: 25 April 2017

present in Fig. 4. The solid line displays the function: $D(\eta,1/U_c)=\eta^2-4(1-1/U_c)=0$. Along the line, we have $\eta^2=4(1-1/U_c)$, and thus $\lambda_{\pm}=-\eta/2$. In other word, the roots are equal and real, and thus the solution is a stable inflected node displayed by a solid circle in Fig. 4. As $D(\eta,1/U_c)>0$ or $\eta^2>4(1-1/U_c)$, the roots are both real and negative. The solution shows no oscillation and thus is a stable node shown by a solid square in Fig. 4. As $D(\eta,1/U_c)<0$ or $\eta^2<4(1-1/U_c)$, the roots are complex with negative real part. This results in oscillations of exponentially decaying amplitude. The solution is a stable spiral or a stable focus shown by an open circle in Fig. 4.

4. Numerical Simulations

Let $y_1=U$ and thus $y_2=dU/d\tau$. Eq. (6) can be re-written as two first-order differential equations:

$$dy_1/d\tau=y_2 \qquad (12a)$$

$$dy_2/d\tau=-y_1-\eta y_2-\exp(-y_1/U_c)+\Gamma_D. \qquad (12b)$$

Eq. (12) will be numerically solved using the fourth-order Runge-Kutta method (Press et al., 1986). To simplify the following computations, the value of Γ_D is set to be a small constant of 10^{-5}, which can continuously enforce the slider to move.

A phase portrait, denoted by y=f(x), is a plot of a physical quantity versus another of an object in a dynamical system (Thompson and Stewart, 1986). The intersection point of the bisection line, i.e., y=x, and f(x) is called the fixed point, that is, f(x)=x. If the function f(x) is continuously differentiable in an open domain near a fixed point x_f and $|f'(x_f)|<1$, attraction is generated. In other words, an attractive fixed point is a fixed point x_f of a function f(x) such that for any value of x in the domain that is close enough to x_f, the iterated function sequences, i.e., x, f(x), $f^2(x)$, $f^3(x)$,…, converges to x_f. An attractive fixed point is a special case of a wider mathematical concept of attractors. Chaos can be generated at some attractors. The details can be seen in Thompson and Stewart (1986) or other nonlinear literatures. In the following plots, the intersection points of the bisection line (denoted by a thin solid line) with the phase portrait of V/V_{max} versus U/U_{max} are the fixed points. To explore nonlinear behavior of a system, the Fourier spectrum $F[V(\Omega_k)]$, where $\Omega_k=k/\delta\tau$ is the

Nonlin. Processes Geophys. Discuss., doi:10.5194/npg-2017-17, 2017
Manuscript under review for journal Nonlin. Processes Geophys.
Discussion started: 25 April 2017

Nonlinear Processes in Geophysics
Discussions
Open Access
EGU

297 dimensionless angular frequency at k=0, ..., N-1, is calculated for the simulation
298 velocity waveform through the fast Fourier transform (Press et al., 1986). The
299 bifurcation from a predominant period to others will be seen in the Fourier spectra.
300 Numerical simulations for the time variation in V/V_{max}, the phase portrait of
301 V/V_{max} versus U/U_{max}, and Fourier spectrum based on different values of model
302 parameters are displayed in Figs. 5–12. In the figures, V_{max} and U_{max} are, respectively,
303 the maximum velocity and displacement for case (a) of each figure, because the
304 maximum values of U and V decrease from case (a) to case (d) in this study.
305 First, the cases excluding viscosity, i.e., $\eta=0$, are explored. Fig. 5 is numerically
306 made for four values of U_c: (a) for $U_c=0.1$; (b) for $U_c=0.4$; (c) for $U_c=0.7$; and (d) for
307 $U_c=0.9$ when $\eta=0$. Fig. 6 is numerically made for four values of U_c: (a) for $U_c=1.00$;
308 (b) for $U_c=1.01$; (c) for $U_c=1.15$; and (d) for $U_c=2.00$ when $\eta=0$. A comparison
309 between Fig. 5 and Fig. 6 suggests that $U_c=1$ is a transition value of the friction law
310 between two modes of slip as displayed in Fig. 4. Only $U_c<1$ is considered below.
311 Secondly, the cases including both friction and viscosity are studied. Fig. 7 is
312 numerically made for four values of η: (a) for $\eta=0.20$; (b) for $\eta=0.50$; (c) for $\eta=0.87$;
313 and (d) for $\eta=0.90$ when $U_c=0.20$. Obviously, the time variation in V/V_{max} exhibits
314 cyclic oscillations with a particular period when $\eta<\eta_l=0.86$ and has intermittent slip
315 with shorter periods when $\eta>\eta_l$. Such a phenomenon holds also for $\eta<5.5$.
316 Fig. 8 is numerically made for four values of η: (a) for $\eta=0.46$; (b) for $\eta=0.47$; (c)
317 for $\eta=0.98$; and (d) for $\eta=0.99$ when $U_c=0.55$. The Fourier spectrum is not calculated
318 for case (d), because the velocity becomes negative infinity at a certain time. The time
319 variation in V/V_{max} exhibits cyclic oscillations specified with three main frequencies
320 when $\eta<\eta_l=0.47$. There is intermittency slip with shorter periods when
321 $\eta_l<\eta<\eta_u=0.98$. There are unstable slip when $\eta>\eta_u$. This phenomenon holds also
322 when $0.55<U_c<1$.
323 Four examples for η varying from $\eta<\eta_u$ to $\eta>\eta_u$ for different values of U_c are
324 displayed in Figs. 9–12. Fig. 9 is made for four values of η: (a) for $\eta=0.39$; (b) for
325 $\eta=0.83$; (c) for $\eta=0.84$; and (d) for $\eta=0.85$ when $U_c=0.6$. Fig. 10 is made for four
326 values of η: (a) for $\eta=0.34$; (b) for $\eta=0.71$; (c) for $\eta=0.72$; and (d) for $\eta=0.73$ when
327 $U_c=0.7$. Fig. 11 is made for four values of η: (a) for $\eta=0.25$; (b) for $\eta=0.53$; (c) for
328 $\eta=0.54$; and (d) for $\eta=0.55$ when $U_c=0.8$. Fig. 12 is made for four values of η: (a) for

329 η=0.14; (b) for η=0.35; (c) for η=0.36; and (d) for η=0.37 when U_c=0.9. The Fourier
330 spectrum is not calculated for case (d) in each example, because the velocity becomes
331 negative infinity at a certain time.

332 Fig. 13 exhibits the data points of η_l (with a solid square) and that of η_u (with a
333 solid circle) for several values U_c. The values of η_l and η_u for several values of U_c
334 are given in Table 1. The figure exhibits a stable regime when $\eta \leq \eta_l$, an intermittency
335 or transition regime when $\eta_l < \eta \leq \eta_u$, and unstable regime when $\eta > \eta_u$.
336
337 **5. Discussion**

338 As mentioned above, the natural period of the one-body system at low
339 displacements is $T_o=2\pi/\omega_o=2\pi(m/K)^{1/2}$ in the absence of friction and viscosity and
340 $T_n=2\pi/\omega_n=T_o/[1-T_o^2(\eta^2+4m\gamma)/(4\pi m)^2]^{1/2}$ in the presence of friction and viscosity.
341 Due to $\gamma=1/u_c$ at u=0, T_n increases with decreasing u_c. Obviously, T_n is longer than
342 T_o and increases with η and γ, thus indicating that friction and viscosity both lengthen
343 the natural period of the system.

344 Based on the marginal analysis of the normalized equation of motion, i.e., Eq.
345 (11), the plot of η versus $1/U_c$ is displayed in Fig. 4 which exhibits the phase portrait
346 and root structure of the system. Since η and U_c are both positive, only the plot of η
347 versu $1/U_c$ in the first quadrant is displayed. In Fig. 4, the solid line displays the
348 function: $D(\eta,1/U_c)=\eta^2-4(1-1/U_c)=0$. Along the line, the solution $\lambda_{\pm}=-\eta/2$ and thus
349 $\exp(\lambda t)=\exp(-\eta/2)$. In other word, the roots are equal and real, and, thus, the phase
350 portrait is a stable inflected node displayed by a solid circle in Fig. 4. Because of $\eta \geq 0$,
351 we have $1/U_c \leq 1$. As $D(\eta,1/U_c)>0$ or $\eta^2>4(1-1/U_c)$, the roots are both real and
352 negative. The solution shows no oscillation and thus phase portrait is a stable node
353 shown by a solid square in Fig. 4. Because of $\eta \geq 0$, we have $1/U_c \leq 1$. As $D(\eta,1/U_c)<0$
354 or $\eta^2<4(1-1/U_c)$, the roots are complex with a negative real part. This results in
355 oscillations with exponentially decaying amplitude. The phase portrait is a stable
356 spiral or a stable focus shown by an open circle in Fig. 4.

357 Fig. 5 exhibits the time variation in V/V_{max}, the phase portrait of V/V_{max} versus
358 U/U_{max}, and Fourier spectrum for four values of U_c: (a) for U_c=0.1; (b) for U_c=0.4; (c)
359 for U_c=0.7; and (d) for U_c=0.9 when η=0. In the first panels, the time variation in
360 V/V_{max} exhibits cyclic behavior and the amplitude of V/V_{max} decreases and the

Nonlin. Processes Geophys. Discuss., doi:10.5194/npg-2017-17, 2017
Manuscript under review for journal Nonlin. Processes Geophys.
Discussion started: 25 April 2017

predominant period of signal increases with increasing U_c. This is consistent with Eq. (5) in which T_n increases with U_c. Although the four phase portraits are almost similar, yet their size decreases with increasing U_c. The second panels exhibit two fixed points: one at V=0 and U=0 and the second one at larger V and larger V. The slope values at the first fixed points decrease with increasing U_c, thus suggesting that the fixed point is not an attractor for small U_c and can be an attractor for larger U_c. The slope values at the fixed points for smaller U_c are greater than 1 and thus they cannot be an attractor. The third panel for each case displays the Fourier spectrum. Fourier spectra exhibit that in addition to the peak related to the predominant frequency, there are numerous peaks associated with higher frequencies. This shows nonlinear behavior caused by nonlinear friction. The frequency related to the first peak decreases with increasing U_c. The amplitude of a peak decreases with increasing U_c. The amplitude of a peak decreases with increasing Ω for small U_c; while it first increases up to the maximum and then decreases with increasing Ω for large U_c. The amplitude of a peak becomes very small when Ω>0.25.

Fig. 6 exhibits the time variation in V/V_{max}, the phase portrait of V/V_{max} versus U/U_{max}, and Fourier spectrum for four values of U_c: (a) for U_c=1.00; (b) for U_c=1.01; (c) for U_c=1.15; and (d) for U_c=2.0 when η=0. In the first panels, the time variation in V/V_{max} exhibits cyclic behavior and the amplitude of V/V_{max} remarkably decreases with increasing U_c when U_c>1. In the second panels, the size of phase portrait decreases with increasing U_c and there are two fixed points: the first one at V=0 and U=0 and the second one at larger V and larger V. With comparison to the phase portrait of U_c=1.0, the phase portrait becomes very small when $U_c \geq 1.15$. In contrast to Fig. 5, the absolute values of slope at the fixed points in Fig. 6 increase with U_c. Hence, the fixed points cannot be an attractor for $U_c \geq 1$. In the third panels, Fourier spectra exhibit that except for U_c=1, there is only one peak and the predominant frequency increases or the predominant period decreases with increasing U_c. This is consistent with Eq. (5). Results show that nonlinear behavior disappears when U_c>1. In addition, the amplitude of a peak decreases with increasing U_c when U_c>1. Obviously, U_c=1 is the critical value of the friction law as displayed in Fig. 4.

Fig. 7 exhibits the time variation in V/V_{max}, the phase portrait of V/V_{max} versus U/U_{max}, and Fourier spectrum for four values of η: (a) for η=0.20; (b) for η=0.50; (c) for η=0.87; and (d) for η=0.90 when U_c=0.20. In the first panels, the time variation in

394 V/V_{max} exhibits cyclic behavior and the amplitude of V/V_{max} decreases with
395 increasing η. The predominant period of signal only slightly increases with increasing
396 η, because η changes in a small range. In the second panels, the size of phase portrait
397 decreases with increasing U_c and there are two fixed points: the first one at V=0 and
398 U=0 and the second one at larger V and larger V. Since the slope values of fixed
399 points are clearly all higher than 1, they are not an attractor. In the third panels, the
400 Fourier spectra exhibit that in addition to the peak related to the predominant
401 frequency, there are numerous peaks associated with higher Ω. This shows nonlinear
402 behavior, mainly caused by nonlinear friction, of the model. The highest peak for case
403 (a) appears at the second frequency. When $\eta<0.9$, the amplitude of a peak decreases
404 with increasing η. The frequencies related to the peaks do not change remarkably,
405 because η varies in a small range. Except for case (a), the amplitude of a peak
406 decreases with increasing Ω. The third peak amplitude disappears when $\eta>0.5$. The
407 amplitude of a peak becomes very small when $\Omega>0.25$. Except for $U_c=0.1$, the
408 frequencies related to the peaks in Fig. 7 are different from and slightly smaller than
409 those in Fig. 5. Note that when $U_c<0.55$ the simulation results in Fig. 5 are similar to
410 those in Fig. 6.

411 Fig. 8 shows the time variation in V/V_{max}, the phase portrait of V/V_{max} versus
412 U/U_{max}, and Fourier spectrum for four values of η: (a) for $\eta=0.46$; (b) for $\eta=0.47$; (c)
413 for $\eta=0.98$; and (d) for $\eta=0.99$ when $U_c=0.55$. When $\eta\leq0.47$, the time variation in
414 V/V_{max} exhibits cyclic oscillations specified with different main angular frequencies.
415 When $\eta>0.47$ (for example $\eta=0.98$ in the figure), in addition to cyclic behavior there
416 is small intermittent slip with shorter periods. This phenomenon also exists when
417 $\eta_l<\eta<\eta_u=0.98$. There are unstable (or chaotic) slip when $\eta>\eta_u$. Hence, the phase
418 portraits in the second panels display unstable slip at small V and U when
419 $\eta_l<\eta\leq\eta_u=0.98$. When $\eta=0.99$, the velocity becomes negative infinity at a certain time
420 and the phase portrait also displays unstable or chaotic slip at small V and U. Since
421 the slope values of fixed points at large V and U are clearly higher than 1, they are not
422 an attractor. Due to the appearance of infinity velocity when $\eta=0.99$, the Fourier
423 spectrum is not calculated for $\eta=0.99$. The Fourier spectra exhibit that when $\eta<0.47$,
424 in addition to the peak related to the predominant frequency, there are numerous peaks
425 associated with higher Ω. This shows nonlinear behavior of the model caused by
426 nonlinear friction. The amplitude of a peak decreases with increasing U_c and the peak

Nonlin. Processes Geophys. Discuss., doi:10.5194/npg-2017-17, 2017
Manuscript under review for journal Nonlin. Processes Geophys.
Discussion started: 25 April 2017

amplitude decreases with increasing Ω. When η=0.98, the amplitude of the highest peak is much larger than others. For the first three cases, the amplitude of a peak becomes very small when Ω>0.25. The frequencies related to the peaks in Fig. 8 are different from and slightly smaller than those in Fig. 7.

Figs. 9–12 show a variation from stable slip to intermittent slip and then to unstable or chaotic slip when η increases from a smaller value to a larger one for U_c=0.6, 0.7, 0.8, and 0.9. The values of η_u for U_c=0.20–0.95 with a unit difference of 0.05 are given in Table 1. Like Fig. 8, when $\eta \le \eta_l$, the time variation in V/V_{max} exhibits only cyclic oscillations specified with different frequencies. When $\eta_l < \eta \le \eta_u$, there are small intermittent displacements appear in the cyclic oscillations. Hence, the phase portraits display that unstable slip at small V and U when $\eta_l < \eta \le \eta_u$. When $\eta > \eta_u$, the velocity becomes negative infinity at a certain time and the phase portrait displays unstable slip at small V and U. Due to the appearance of infinity velocity, the Fourier spectrum is not calculated for $\eta > \eta_u$. When $\eta < \eta_l$, in addition to the peak related to the predominant frequency, there are numerous peaks related to higher Ω. This shows nonlinear behavior, mainly caused by nonlinear friction, of the model. The amplitude of a peak decreases with increasing U_c and the amplitude of a peak decreases with increasing Ω. For the first three cases, the amplitude of a peak becomes very small when Ω>0.25. Figs. 7–12 show that the frequencies related to the peaks slightly decrease with increasing U_c and the decreasing rate decreases with increasing U_c. In other word, the frequencies related to the peaks for large U_c are almost similar. The number of higher peaks and the amplitudes of peaks at higher Ω both decrease with increasing η. This indicates that viscosity makes a stronger effect on higher- frequency waves than on lower ones, and the effect increases with η.

Fig. 13 exhibits the data points of η_l (with a solid square) and that of η_u (with a solid circle) for several values U_c. The values of η_l and η_u for several values of U_c are given in Table 1. The figure exhibits a stable regime when $\eta \le \eta_l$, an intermittency (or transition) regime when $\eta_l < \eta \le \eta_u$, and unstable (or chaotic) regime when $\eta > \eta_u$. When U_c<0.55, there is no η_l, in other word, unstable slip does not exist. Clearly, η_l, η_u, and their difference η_u-η_l all decrease with increasing U_c. This means that it is easier to yield unstable slip for larger U_c than for smaller U_c. Since smaller U_c is associated to larger γ of decreasing rate of friction force with slip, it is easier to yield

459 unstable slip from smaller γ than from larger γ.

460 Huang and Turcotte (1990, 1992) observed intermittent phases in the
461 displacements based on a two-body model. In other word, some major events are
462 proceeded by numerous small events. Those small events could be foreshocks. They
463 also claimed that earthquakes are an example of deterministic chaos. Ryabov and Ito
464 (2001) also found intermittent phase transitions in a two-dimensional one-body model
465 with velocity-weakening friction. Their simulations exhibit that intermittent phases
466 appear before large ruptures. From numerical simulations of earthquake ruptures
467 using a one-body model with a rate- and state-friction law, Erickson et al. (2008)
468 found that the system undergoes a Hopf bifurcation to a periodic orbit. This periodic
469 orbit then undergoes a period doubling cascade into a strange attractor, recognized as
470 broadband noise in the power spectrum. From numerical simulations of earthquake
471 ruptures using a two-body model with a rate- and state-friction law, Abe and Kato
472 (2013) observed various slip patterns, including the periodic recurrence of seismic and
473 aseismic slip events, and several types of chaotic behavior. The system exhibits
474 typical period-doubling sequences for some parameter ranges, and attains chaotic
475 motion. Their results also suggest that the simulated slip behavior is deterministic
476 chaos andt ime variations of cumulative slip in chaotic slip patterns can be well
477 approximated by a time-predictable model. In some cases, both seismic and aseismic
478 slip events occur at a slider, and aseismic slip events complicate the earthquake
479 recurrence patterns. The present results seem to be comparable with those made by
480 the previous authors, even though viscosity was not included in their studies. This
481 suggests that nonlinear friction and viscosity play the first and second roles,
482 respectively, on the intermittent phases. The intermittent phases could be considered
483 as foreshocks of the mainshock which is associated with the main rupture. Simulation
484 results exhibit that foreshocks happen for some mainshcoks and not for others.
485

486 **6. Conclusions**

487 In this work, multistable slip of earthquakes caused by slip-weakening friction
488 and viscosity is studied based on the normalized equation of motion of a one-degree-
489 of-freedom spring-slider model in the presence of the two factors. The friction is
490 caused by thermal pressurization and decays exponentially with displacement. The
491 major model parameters are the normalized characteristic distance, U_c, for friction

and the normalized viscosity coefficient, η, between the slider and the background moving plate, which exerts a driving force on the former. Analytic results at small U suggest that there is a solution regime for η and γ ($=1/U_c$) to make the slider slip steadily. Numerical simulations lead to the time variation in V/V_{max}, the phase portrait of V/V_{max} versus U/U_{max}, and Fourier spectrum. Results show that the time variation in V/V_{max}, obviously depends on U_c and η. The effect on the amplitude is stronger from η than from U_c. When $U_c>1$, the time variation of V/V_{max} exhibits cyclic oscillations with a single period and the amplitude of V/V_{max} remarkably decreases with increasing U_c. When $U_c<1$, slip changes from stable motion to intermittency and then to unstable motion when η increases. For a certain U_c, the three regimes are controlled by a lower bound, η_l, and an upper bound, η_u, of η. When $U_c<0.55$, η_u is absent and thus unstable or chaotic slip does not exist. When $U_c\geq0.55$, the plots of η_l and η_u versus U_c exhibit a stable regime when $\eta\leq\eta_l$, an intermittency (or transition) regime when $\eta_l<\eta\leq\eta_u$, and unstable (or chaotic) regime when $\eta>\eta_u$. The values of η_l, η_u, and η_u-η_l all decrease with increasing U_c, thus suggesting that it is easier to yield unstable slip for larger U_c than for smaller U_c or larger η than for smaller η. The phase portraits of V/V_{max} versus U/U_{max} exhibit that there are two fixed points: The first one at large V/V_{max} and large U/U_{max} is not an attractor for all cases in study; while the second one at small V/V_{max} and small U/U_{max} can be an attractor for some values of U_c and η. When $U_c<1$, the Fourier spectra calculated from simulation velocity waveforms exhibit several peaks rather than one, thus suggesting the existence of nonlinear behavior of the system. When $U_c>1$, the related Fourier spectra show only one peak, thus suggesting linear behavior of the system.

Acknowledgments. The study was financially supported by Academia Sinica, the Ministry of Science and Technology (Grant No.: MOST-105-2116-M-001-007), and the Central Weather Bureau (Grant No.: MOTC-CWB-106-E-02).

References

Abe, Y. and N. Kato (2013). Complex earthquake cycle simulations using a two-degree-of-freedom spring-block model with a rate- and state-friction law. Pure Appl. Geophys., 170, 745-765.

Belardinelli, M.E. and E. Belardinelli (1996). The quasi-static approximation of the

525 spring-slider motion. Nonl. Process Geophys., 3, 143-149.
526 Bizzarri, A. (2009). What does control earthquake ruptures and dynamic faulting? A
527 review of different competing mechanism. Pure Appl. Geophys., 166, 741-776.
528 Bizzarri, A. (2010). An efficient mechanism to avert frictional melts during seismic
529 ruptures. Earth Planet. Sci. Lett., 296, 144-152, doi:10.1016/j.epsl.2010.05.012.
530 Bizzarri, A. (2011a). Dynamic seismic ruptures on melting fault zones. J. Geophys.
531 Res., 116, B02310, doi:10.1029/2010JB007724.
532 Bizzarri, A. (2011b). Temperature variations of constitutive parameters can
533 significantly affect the fault dynamics. Earth Planet. Sci. Lett., 306, 72-278, doi:
534 10.1016/j.epsl.2011.04.009.
535 Bizzarri, A. (2011c). On the deterministic description of earthquakes. Rev. Geophys.,
536 49, RG3002, doi:10.1029/2011RG000356.
537 Bizzarri, A. and M. Cocco (2006a). A thermal pressurization model for the
538 spontaneous dynamic rupture propagation on a three-dimensional fault: 1.
539 Methodological approach. J. Geophys. Res., 111, B05303, doi:10.1029/
540 2005JB003862.
541 Bizzarri, A. and M. Cocco (2006b). A thermal pressurization model for the
542 spontaneous dynamic rupture propagation on a three-dimensional fault: 2.
543 Traction evolution and dynamic parameters. J. Geophys. Res., 111, B05304,
544 doi:10.1029/2005JB003864.
545 Brun, J.L. and A.B. Gomez (1994). A four-parameter, two degree-of-freedom
546 block-spring model: Effect of the driver velocity. Pure Appl. Geophys., 143(4),
547 633-653
548 Burridge, R. and L. Knopoff (1967). Model and theoretical seismicity. Bull. Seism.
549 Soc. Am., 57, 341-371.
550 Byerlee, J.D. (1968). Brittle-ductile transition in rocks. J. Geophys. Res., 73,
551 4711-4750.
552 Carlson, J.M. and J.S. Langer (1989). Mechanical model of an earthquake fault. Phys.
553 Rev. A, 40, 6470-6484.
554 Chester, F.M., and H.G. Higgs (1992). Multimechanism friction constitutive model
555 for ultrafine quartz gouge at hypocentral conditions. J. Geophys. Res., 97, B2,
556 1859-1870.
557 Cohen, S. (1979). Numerical and laboratory simulation of fault motion and
558 earthquake occurrence. Rev. Geophys. Space Phys., 17(1), 61-72.

559 Diniega, S., S.E. Smrekar, S. Anderson, and E.R. Stofan (2013). The influence of
560 temperature-dependent viscosity on lava flow dynamics. J. Geophys. Res., 118,
561 1516-1532, doi:10.1002/jgrf.20111.

562 Dragoni, M. and S. Santini (2015). A two-asperity fault model with wave
563 radiation. Phys. Earth Planet. Inter., 248, 83-93.

564 Erickson, B., B. Birnir1, and D. Lavall´ee (2008). A model for aperiodicity in
565 earthquakes. Nonlin. Process Geophys., 15, 1-12.

566 Erickson, B.A., B. Birnir, and D. Lavall´ee (2011). Periodicity, chaos and localization
567 in a Burridge–Knopoff model of an earthquake with rate-and-state friction.
568 Geophys. J. Int., 187, 178-198, doi:10.1111/j.1365-246X.2011.05123.x.

569 Fialko, Y.A. (2004). Temperature fields generated by the elastodynamic propagation
570 of shear cracks in the Earth. J. Geophys. Res., 109, B01303, doi:10.1029/
571 2003JB002496.

572 Fialko, Y.A. and Y. Khazan (2005). Fusion by the earthquake fault friction: stick or
573 slip?. J. Geophys. Res., 110, B12407, doi.org/10.1029/2005JB003869.

574 Galvanetto, U. (2002). Some remarks on the two-block symmetric Burridge–Knopoff
575 model. Phys. Letts. A, 251-259.

576 Gu, J.C., J.R. Rice, A.L. Ruina, and S.T. Tse (1984). Slip motion and stability of a
577 single degree of freedom elastic system with rate and state dependent friction. J.
578 Phys. Solid, 32, 167-196.

579 Huang, J. and D.L. Turcotte (1990). Are earthquakes an example of deterministic
580 chaos?. Geophys. Res. Lett., 17(3), 223-226.

581 Huang, J. and D.L. Turcotte (1992). Chaotic seismic faulting with a mass-spring
582 model and velocity-weakening friction. Pure Appl. Geophys., 138(4), 549-589.

583 Hudson, J.A. (1980). The excitation and propagation of elastic waves. Cambridge
584 Monographs on Mechanics and Applied Mathematics, Cambridge Univ. Press,
585 224pp.

586 Jaeger, J.C. and N.G.W. Cook (1977). Fundamentals of Rock Mechanics. John Wiley
587 & Sons, Inc., New York, 585pp.

588 Jeffreys, H. (1942). On the mechanics of faulting. Geol. Mag., 79, 291.

589 Kittel, C., W.D. Knight, and M.A. Ruderman (1968). Mechanics, Berkeley Physics
590 Course Volume 1, McGraw-Hill Book Co., New York, N.Y., 480pp.

591 Knopoff, L. and X.X. Ni (2001). Numerical instability at the edge of a dynamic
592 fracture. Geophys. J. Int., 147, F1-F6.
593 Knopoff, L., J.Q. Mouton, and R. Burridge (1973). The dynamics of a one-
594 dimensional fault in the presence of friction. Geophys. J. R. astro. Soc., 35,
595 169-184.
596 Kostić, S., I. Franović, K. Todorović, and N. Vasovi (2013). Friction memory effect
597 in complex dynamics of earthquake model. Nonlin. Dyn., 73, 1933-1943, DOI:10.
598 1007/s11071-013-0914-8.
599 Lachenbruch, A.H. (1980). Frictional heating, fluid pressure, and the resistance to
600 fault motion. J. Geophys. Res., 85, 6097-6122.
601 Lorenz, E.N. (1963). Deterministic non-periodic flow. J. Atmos. Sci., 20(2), 130-141.
602 Lu, X., A.J. Rosakis, and N. Lapusta (2010). Rupture modes in laboratory earthquakes:
603 Effect of fault prestress and nucleation conditions. J. Geophys. Res., 115,
604 B12302, doi:10.1029/2009JB006833.
605 Nussbaum, J. and A. Ruina (1987). A two degree-of-freedom earthquake model with
606 static/dynamic friction. Pure Appl. Geophys., 125(4), 629-656.
607 Parez Pascual, R. and J. Lomnitz-Adler (1988). Coupled relaxation oscillators and
608 circle maps. Physica D, 30, 61-82.
609 Press, W.H., B.P. Flannery, S.A. Teukolsky, and W.T. Vetterling (1986). Numerical
610 Recipes. Cambridge Univ. Press, Cambridge, 818pp.
611 Rice, J.R. (2006). Heating and weakening of faults during earthquake slip. J. Geophys.
612 Res., 111, B05311, doi:10.1029/2005JB004006.
613 Rice, J.R., N. Lapusta, and K. Ranjith (2001). Rate and state dependent friction and
614 the stability of sliding between elastically deformable solids. J. Mech. Phys.
615 Solids, 49, 1865-1898.
616 Ryabov, V.B. and K. Ito (2001). Intermittent phase transitions in a slider-spring
617 model as a mechanism for earthquakes. Pure Appl. Geophys., 158, 919-930.
618 Scholz, C.H. (1990). The Mechanics of Earthquakes and Faulting. Cambridge Univ.
619 Press, Cambridge, 439pp.
620 Sibson, R.H. (1973). Interaction between temperature and pore-fluid pressure during
621 earthquake faulting and a mechanism for partial or total stress relief. Natural
622 Phys. Sci., 243, 66-68.
623 Shkoller and Minster (1997). Reduction of Dieterich-Ruina attractors to unimodal
624 maps. Nonl. Process Geophys., 4, 63-69.

de Sousa Vieira, M. (1999). Chaos and synchronized chaos in an earthquake model. Phys. Rev. Letts., 82(1), 201-204.

Spray, J.G. (1993). Viscosity determinations of some frictionally generated silicate melts: Implications for fault zone rheology at high strain rates. J. Geophys. Res., 98(B5), 8053-8068.

Spray, J.G. (1995). Pseudotachylyte controversy: Fact or friction?. Geology, 23(12), 1119-1122.

Spray, J.G. (2005). Evidence for melt lubrication during large earthquakes. Geophys. Res. Lett., 32, L07301, doi:10.1029/2004GL022293.

Thompson, J.M.T. and H.B. Stewart (1986). Nonlinear Dynamics and Chaos. John Wiley and Sons, New York, 376pp.

Turcotte, D.L. (1992). Fractals and chaos in geology and geophysics. Cambridge Univ. Press, London, 221pp.

Turcotte, D.L. and G. Schubert (1982). GEODYNAMICS – Applications of Continuum Physics to Geological Problems. Wiley, 450pp.

Wang, J.H. (1995). Effect of seismic coupling on the scaling of seismicity. Geophys. J. Int., 121, 475-488.

Wang, J.H. (1996). Velocity-weakening friction law as a factor in controlling the frequency-magnitude relation of earthquakes. Bull. Seism. Soc. Am., 86, 701-713.

Wang, J.H. (2000). Instability of a two-dimensional dynamical spring-slider model of an earthquake fault. Geophys. J. Int., 143, 389-394.

Wang, J.H. (2006). Energy release and heat generation during the 1999 Chi-Chi, Taiwan, earthquake. J. Geophys. Res., 111, B11312, doi:10.1029/2005JB004018.

Wang, J.H. (2007). A dynamic study of the frictional and viscous effects on earthquake rupture: a case study of the 1999 Chi-Chi earthquake, Taiwan. Bull. Seism. Soc. Am., 97(4), 1233-1244.

Wang, J.H. (2008). One-dimensional dynamical modeling of earthquakes: A review, Terr. Atmos. Ocean. Sci., 19, 183-203.

Wang, J.H. (2009). Effect of thermal pressurization on the radiation efficiency. Bull. Seism. Soc. Am., 99(4), 2293-2304.

Wang, J.H. (2011). Thermal and pore fluid pressure history on the Chelungpu fault at a depth of 1111 meters during the 1999 Chi-Chi, Taiwan, earthquake. J. Geophys. Res., 116, B03302, doi:10.1029/2010JB007765.

659 Wang, J.H. (2012). Some intrinsic properties of the two-dimensional
660 dynamical spring-slider model of earthquake faults. Bull. Seism. Soc. Am.,
661 102(2), 822-835.
662 Wang, J.H. (2013). Stability analysis of slip of a one-body spring-slider model in the
663 presence of thermal pressurization. Ann. Geophys., 56(3), R03332, doi:10.4401/
664 ag-5548.
665 Wang, J.H. (2016a). A dynamical study of frictional effect on scaling of earthquake
666 source displacement spectra. Ann. Geophys., 59(2), S0210, 1-14, doi:10.4401/
667 ag-6974.
668 Wang, J.H. (2016b). Slip of a one-body spring-slider model in the presence of
669 slip-weakening friction and viscosity. Ann. Geophys., 59(5), S0541, DOI:10.
670 4401/ag-7063.
671 Wang, J.H. (2017). Slip of a two-degree-of-freedom spring-slider model in the
672 presence of slip-weakening friction and viscosity., Ann. Geophys. (in press)
673 Xu, H.J. and L. Knopoff (1994). Periodicity and chaos in a one-dimensional
674 dynamical model of earthquakes. Phys. Rev. E, 50(5), 3577-3581.
675
676

Nonlin. Processes Geophys. Discuss., doi:10.5194/npg-2017-17, 2017
Manuscript under review for journal Nonlin. Processes Geophys.
Discussion started: 25 April 2017

Nonlinear Processes in Geophysics
Discussions
Open Access
EGU

677
678
679
680 Table 1. Values of η_l, η_u, and V_{max} for various U_c.

U_c	η_l	η_u	V_{max}
0.20	0.87	1.00	0.4068
0.25	0.86	1.00	0.3611
0.30	0.86	1.00	0.3149
0.35	0.77	1.00	0.2905
0.40	0.69	1.00	0.2649
0.45	0.57	1.00	0.2497
0.50	0.51	1.00	0.2216
0.55	0.43	0.98	0.1989
0.60	0.39	0.84	0.1684
0.65	0.38	0.78	0.1338
0.70	0.34	0.72	0.1071
0.75	0.26	0.69	0.0879
0.80	0.25	0.55	0.0604
0.85	0.18	0.48	0.0423
0.90	0.14	0.37	0.0234
0.95	0.12	0.25	0.0076

681
682

Nonlin. Processes Geophys. Discuss., doi:10.5194/npg-2017-17, 2017
Manuscript under review for journal Nonlin. Processes Geophys.
Discussion started: 25 April 2017

683

684

685

686

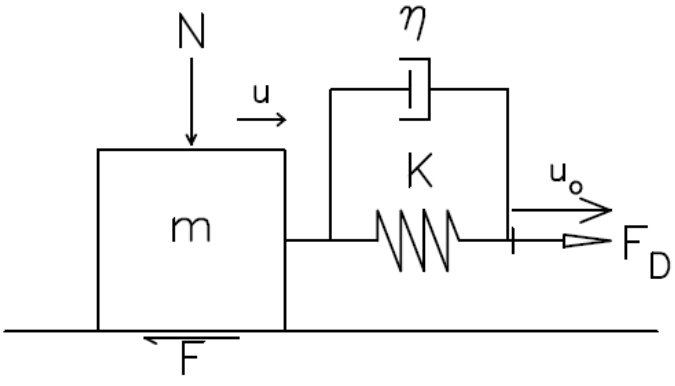

687

688 Figure 1. One-body spring-slider model. In the figure, u, K, η, F_D, N, and F denote,
689 respectively, the displacement, the spring constant, the viscosity coefficient, the
690 driving force, the normal force, and the frictional force.

691

692

Nonlin. Processes Geophys. Discuss., doi:10.5194/npg-2017-17, 2017
Manuscript under review for journal Nonlin. Processes Geophys.
Discussion started: 25 April 2017

693

694

695

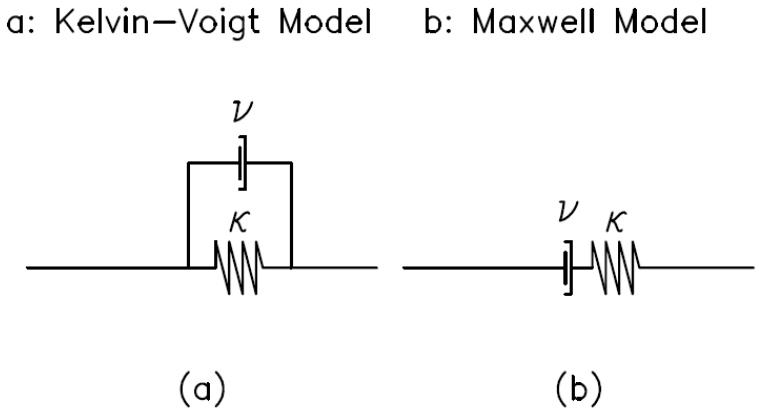

696

697 Figure 2. The two types of viscous materials: (a) for the Kelvin–Voigt model and (b)
698 for the Maxwell model. (κ=spring constant and υ=coefficient of viscosity)
699

700

Nonlin. Processes Geophys. Discuss., doi:10.5194/npg-2017-17, 2017
Manuscript under review for journal Nonlin. Processes Geophys.
Discussion started: 25 April 2017

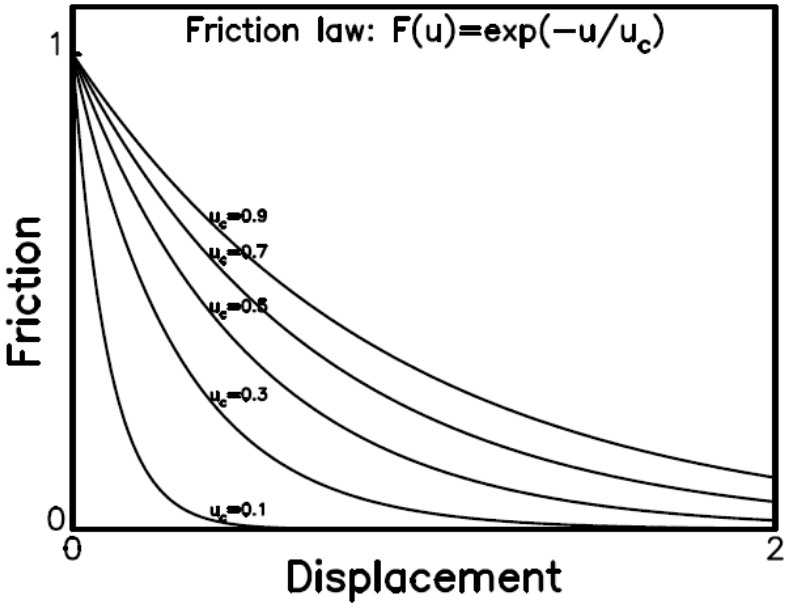

Figure 3. The variations in friction force with displacement for $F(u)=\exp(-u/u_c)$ when u_c=0.1, 0.3, 0.5, 0.7, and 0.9 m (after Wang, 2016b).

Nonlin. Processes Geophys. Discuss., doi:10.5194/npg-2017-17, 2017
Manuscript under review for journal Nonlin. Processes Geophys.
Discussion started: 25 April 2017

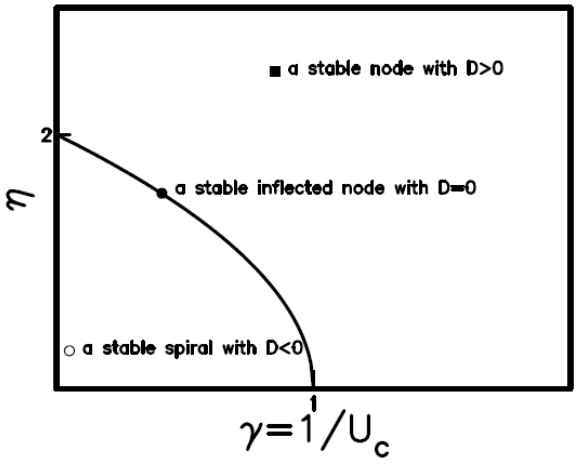

Figure 4. The plot of η versus $1/U_c$ exhibits the phase portrait and root structure of the system. The solid line displays the function: $D(\eta,1/U_c)=\eta^2-4(1-1/U_c)=0$. The solid circle, open circle, and solid square represent, respectively, a stable inflected node with D=0, a stable spiral with D<0, and a stable node with D>0.

Nonlin. Processes Geophys. Discuss., doi:10.5194/npg-2017-17, 2017
Manuscript under review for journal Nonlin. Processes Geophys.
Discussion started: 25 April 2017

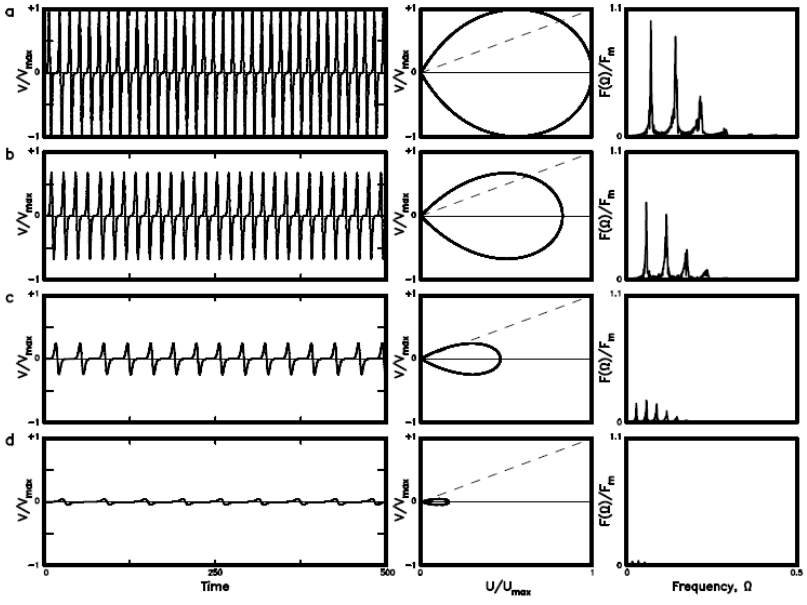

Figure 5. The time variation in V/V_{max}, the phase portrait of V/V_{max} versus U/U_{max}, and power spectrum for four values of U_c: (a) for U_c=0.1; (b) for U_c=0.4; (c) for U_c=0.7; and (d) for U =0.9 for the TP law of $F(U)=\exp(-U/U_c)$ when η=0.

Nonlin. Processes Geophys. Discuss., doi:10.5194/npg-2017-17, 2017
Manuscript under review for journal Nonlin. Processes Geophys.
Discussion started: 25 April 2017

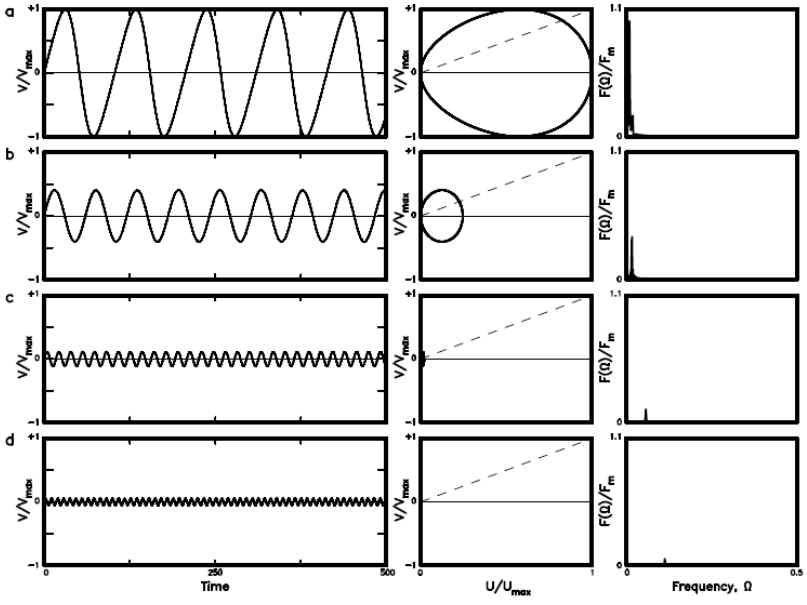

Figure 6. The time variation in V/V_{max}, the phase portrait of V/V_{max} versus U/U_{max}, and power spectrum for four values of U_c: (a) for U_c=1.00; (b) for U_c=1.01; (c) for U_c=1.15; and (d) for U =2.00 for the TP law of $F(U)=\exp(-U/U_c)$ when η=0.

Nonlin. Processes Geophys. Discuss., doi:10.5194/npg-2017-17, 2017
Manuscript under review for journal Nonlin. Processes Geophys.
Discussion started: 25 April 2017

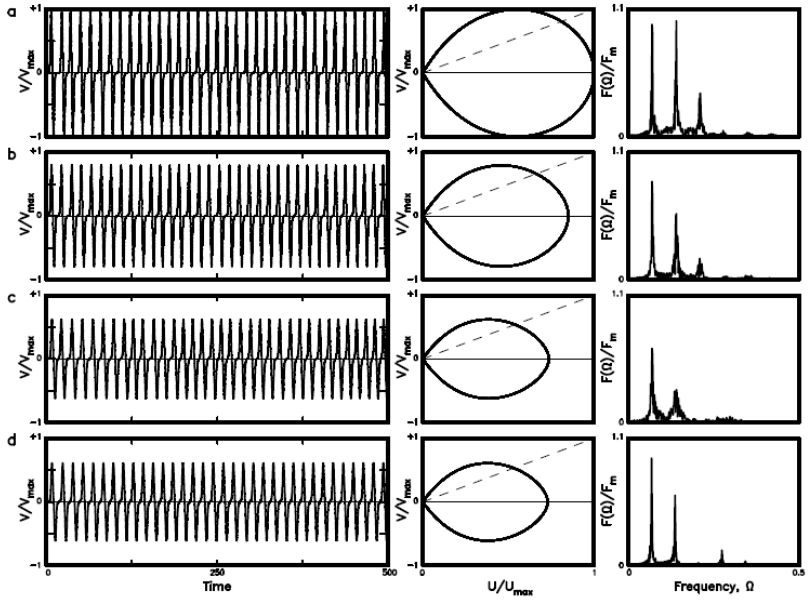

Figure 7. The time variation in V/V_{max}, the phase portrait of V/V_{max} versus U/U_{max}, and power spectrum for four values of η: (a) for η=0.20; (b) for η=0.50; (c) for η=0.87; and (d) for η=0.90 when U_c=0.20 for the TP law of $F(U)=\exp(-U/U_c)$.

Nonlin. Processes Geophys. Discuss., doi:10.5194/npg-2017-17, 2017
Manuscript under review for journal Nonlin. Processes Geophys.
Discussion started: 25 April 2017

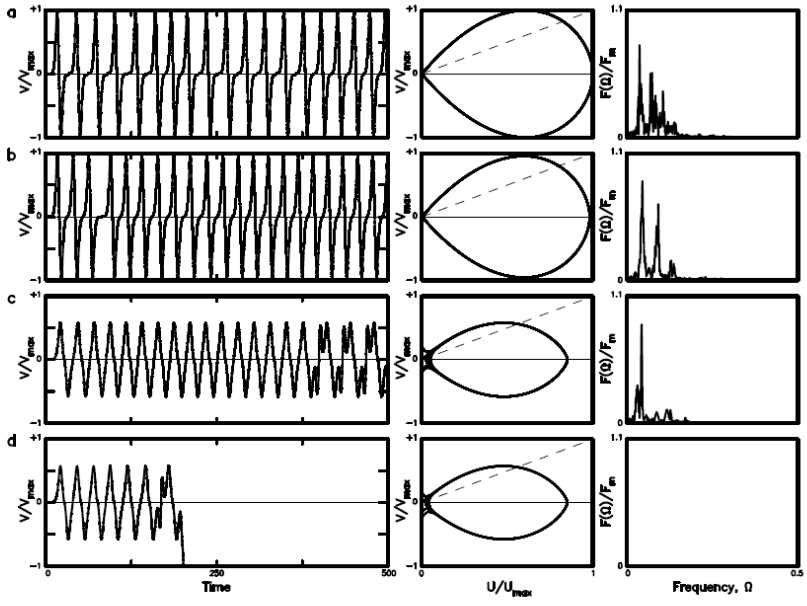

Figure 8. The time variation in V/V_{max}, the phase portrait of V/V_{max} versus U/U_{max}, and power spectrum for four values of η: (a) for η=0.43; (b) for η=0.47; (c) for η=0.98; and (d) for η=0.99 when U_c=055 for the TP law of $F(U)=\exp(-U/U_c)$.

Nonlin. Processes Geophys. Discuss., doi:10.5194/npg-2017-17, 2017
Manuscript under review for journal Nonlin. Processes Geophys.
Discussion started: 25 April 2017

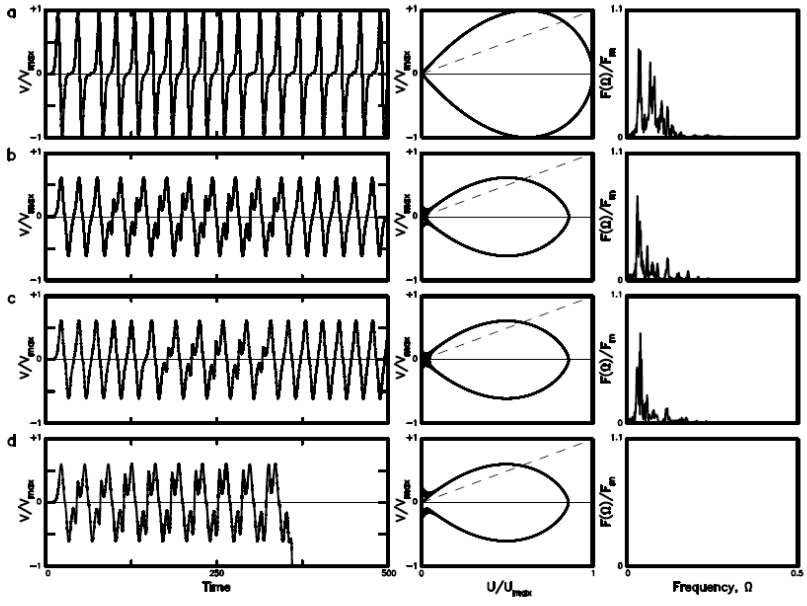

Figure 9. The time variation in V/V_{max}, the phase portrait of V/V_{max} versus U/U_{max}, and power spectrum for four values of η: (a) for η=0.39; (b) for η=0.83; (c) for η=0.84; and (d) for η=0.85 when U_c=0.6 for the TP law of $F(U)=\exp(-U/U_c)$.

Nonlin. Processes Geophys. Discuss., doi:10.5194/npg-2017-17, 2017
Manuscript under review for journal Nonlin. Processes Geophys.
Discussion started: 25 April 2017

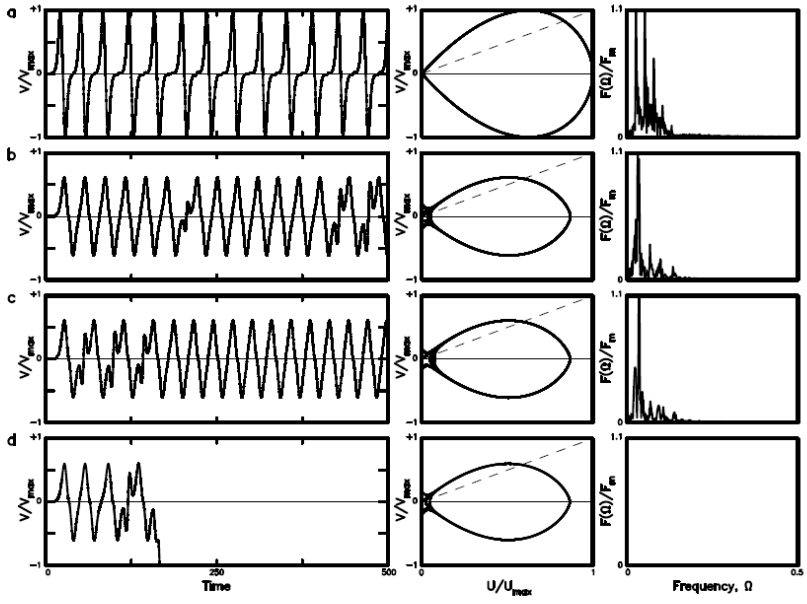

Figure 10. The time variation in V/V_{max}, the phase portrait of V/V_{max} versus U/U_{max}, and power spectrum for four values of η: (a) for η=0.34; (b) for η=0.71; (c) for η=0.72; and (d) for η=0.73 when U_c=0.7 for the TP law of $F(U)=\exp(-U/U_c)$.

Nonlin. Processes Geophys. Discuss., doi:10.5194/npg-2017-17, 2017
Manuscript under review for journal Nonlin. Processes Geophys.
Discussion started: 25 April 2017

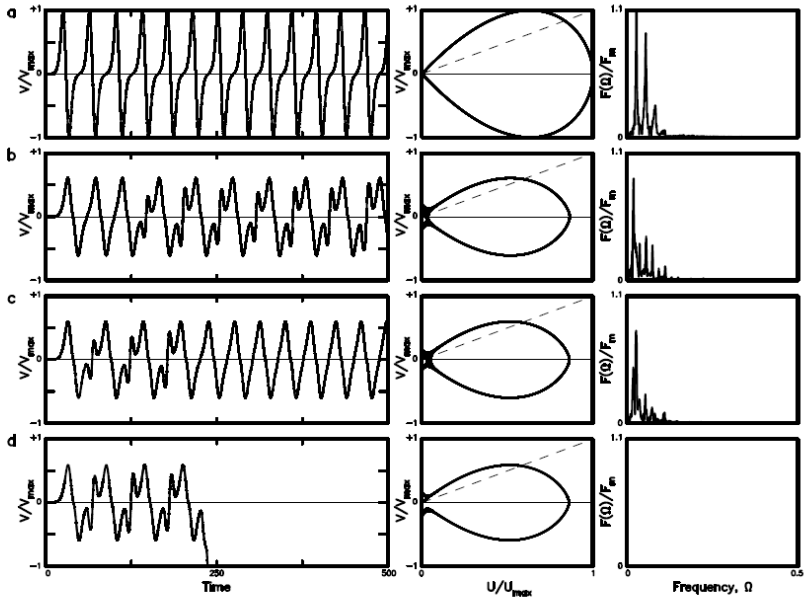

Figure 11. The time variation in V/V_{max}, the phase portrait of V/V_{max} versus U/U_{max}, and power spectrum for four values of η: (a) for η=0.25; (b) for η=0.54; (c) for η=0.55; and (d) for η=0.56 when U_c=0.8 for the TP law of $F(U)=\exp(-U/U_c)$.

Nonlin. Processes Geophys. Discuss., doi:10.5194/npg-2017-17, 2017
Manuscript under review for journal Nonlin. Processes Geophys.
Discussion started: 25 April 2017

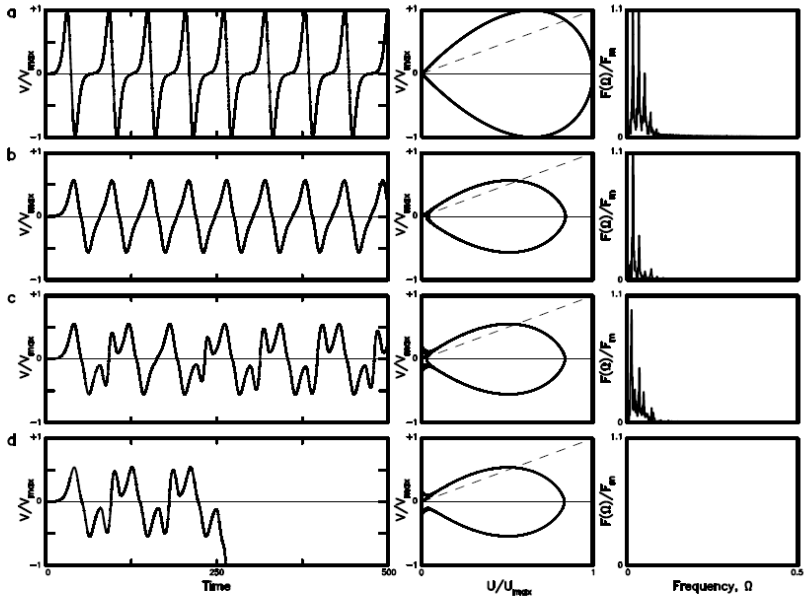

Figure 12. The time variation in V/V_{max}, the phase portrait of V/V_{max} versus U/U_{max}, and power spectrum for four values of η: (a) for η=0.14; (b) for η=0.36; (c) for η=0.37; and (d) for η=0.38 when U_c=0.9 for the TP law of $F(U)=\exp(-U/U_c)$.

Nonlin. Processes Geophys. Discuss., doi:10.5194/npg-2017-17, 2017
Manuscript under review for journal Nonlin. Processes Geophys.
Discussion started: 25 April 2017

792

793

794

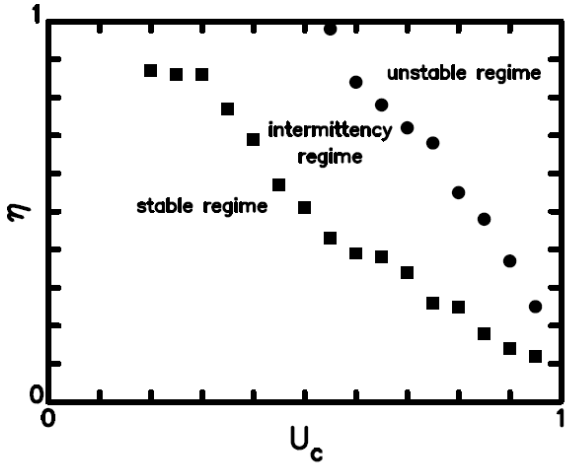

795
796 Figure 13. The plot of η_l (with a solid square) and η_u (with a solid circle) versus U_c.